Experiments in Fluids (2005) 38: 511–515
DOI 10.1007/s00348-005-0942-3

ORIGINALS

H. Nobach · M. Honkanen

Two-dimensional Gaussian regression for sub-pixel displacement estimation in particle image velocimetry or particle position estimation in particle tracking velocimetry

Received: 6 September 2004 / Revised: 20 January 2005 / Accepted: 20 January 2005 / Published online: 17 March 2005

Abstract An explicit solution of two-dimensional Gaussian regression for the estimation of particle displacement from the correlation function in particle image velocimetry (PIV) or particle position from the images in particle tracking velocimetry (PTV) with sub-pixel accuracy is introduced. The accuracy and the ability of the methods to avoid pixel locking due to non-axially orientated, elliptically shaped particle images or correlation peaks are investigated using simulated and experimentally obtained images.

1 Introduction

To increase the accuracy of the displacement estimation in particle image velocimetry (PIV) or the particle position estimation in particle tracking velocimetry (PTV) beyond the resolution given by the size of the sensor elements (pixel), interpolation methods are used which yield the maximum location of the cross-correlation peak in the cross-correlation function or the particle position from the image with sub-pixel accuracy (Willert and Gharib 1991).

Assuming circular or elliptical, axially orientated particle images, the interpolation task can be separated into two one-dimensional interpolations. In PIV and PTV processing, the peak centroid (Morgan et al. 1989; Alexander and Ng 1991):

$$\Delta x = \frac{z_{X+1} - z_{X-1}}{z_{X-1} + z_X + z_{X+1}} \tag{1}$$

and the Gaussian interpolation (Willert and Gharib 1991):

$$\Delta x = \frac{\ln(z_{X-1}) - \ln(z_{X+1})}{2[\ln(z_{X+1}) - 2\ln(z_X) + \ln(z_{X-1})]} \tag{2}$$

based on the maximum sample z_X of a local image area or the correlation function and the two neighbors z_{X-1} and z_{X+1} are widely used. The maximum of the interpolated curve is located at Δx with respect to the index X of the maximum sample (Fig. 1a). The interpolation in the y direction reads similar. While the first method yields a strong fractional displacement towards integer values, which is known as pixel or peak locking (Prasad et al. 1992), the latter method works exactly for ideally Gaussian-shaped particle images or correlation peaks, and, therefore, it became the standard in PIV and PTV processing.

The quality decreases with influences of the diffraction-limited lens (Adrian and Yao 1985), which yields an Airy intensity function for small particles and circular apertures, or the intensity integration over the sensor areas (Westerweel 1997; Huang et al. 1997; Marxen et al. 2000). Both influences can be reduced with more accurate imaging models, namely, the point spread function of the camera objective convolved with the sensitivity distribution of the sensor element. Unfortunately, this requires the optical parameters to be known very accurately, which is difficult in experimental environments. Alternative interpolation schemes such as the Whittaker sinc interpolation (Lourenco and Krothapalli 1995; Roesgen 2003) or splines also yield good results, but only if the influence of under-sampling can be neglected. For commonly used particle image diameters between 2 and 3 pixels, this is not fulfilled and the remaining bias is significant (Nobach et al. 2004).

If the values have an offset (Keane and Adrian 1992), which often occurs due to background images or unaccurately calibrated amplifiers, Eq. 2 yields a strong bias,

H. Nobach (✉)
Fachgebiet Strömungslehre und Aerodynamik,
Technische Universität Darmstadt, Petersenstr. 30,
64289 Darmstadt, Germany
E-mail: holger.nobach@nambis.de

M. Honkanen
Energy and Process Engineering,
Tampere University of Technology,
P.O. Box 589, 33101 Tampere, Finland

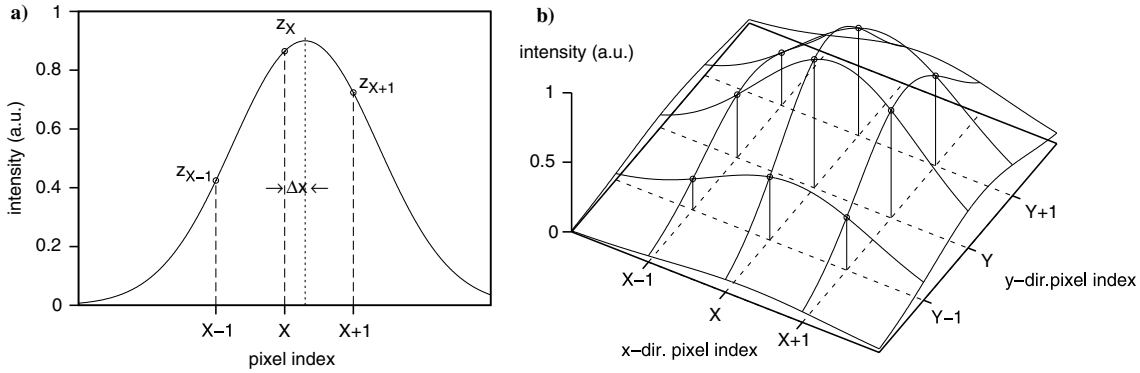

Fig. 1 **a** One-dimensional three-point interpolation and **b** two-dimensional Gaussian regression

which can be reduced by an extended model with an additional constant offset parameter based on four or more intensity values. However, even then, if random intensity fluctuations due to the photon noise or the dark current noise are present, the logarithm in Eq. 2 yields biased estimates due to the value-dependent scaling of the random fluctuations. Note that the noise distribution is different for the image and for the correlation function. To reduce the bias due to the amplitude-dependent scaling, the Gaussian model can be fit directly to the measured values without the logarithm. Furthermore, appropriate weighting schemes and transforms of the measured intensities and the particle image model (e.g., the Fisher transform for the correlation function, Ronneberger et al. (1998)) can be used to obtain a distribution of the random fluctuations, which allows unbiased estimates of the peak location.

However, numerical aberration of the optical lenses can lead to elliptical particle images and elliptically shaped correlation peaks at the edges of the image, which, additionally, are rotated at the image corners (Ronneberger et al. 1998). Here, the two separate one-dimensional, three-point interpolations yield a bias and a significant pixel locking (Fig. 3b), which can be avoided by using a two-dimensional Gaussian fit (Ronneberger et al. 1998). The affecting influence of the noise and the offset can also be decreased here with an extended model, which includes the offset and appropriate transforms and weighting schemes. If high accuracy is required, this method is accepted as an appropriate estimator, even if an explicit solution has not been found and the model fit must be realized as an iterative optimization procedure.

Here, an explicit procedure is introduced which realizes the Gaussian regression by minimizing the L_2 norm of the two-dimensional parabolic fit to the logarithmic values of the correlation function or image intensity, respectively. Unfortunately, the procedure cannot handle an added value. Therefore, it requires image pre-processing to suppress random noise and to remove the image background. According to tests with experimental data, the procedure is able to avoid the pixel locking in the case of elliptically shaped, non-axially oriented particle images or correlation peaks.

2 Gaussian regression

Consider an elliptical Gaussian intensity function:

$$z(x;y) = a\,\exp\{b_{20}(x-\Delta x)^2 + b_{11}(x-\Delta x)(y-\Delta y) + b_{02}(y-\Delta y)^2\} \tag{3}$$

with its maximum at $[\Delta x; \Delta y]$. This can also be expressed as:

$$z(x;y) = \exp\{c_{00} + c_{10}x + c_{20}x^2 + c_{01}y + c_{11}xy + c_{02}y^2\} \tag{4}$$

with:

$$c_{00} = \ln(a) + b_{20}\Delta^2 x + b_{11}\Delta x\Delta y + b_{02}\Delta^2 y \tag{5}$$

$$c_{10} = -2b_{20}\Delta x - b_{11}\Delta y \tag{6}$$

$$c_{20} = b_{20} \tag{7}$$

$$c_{01} = -b_{11}\Delta x - 2b_{02}\Delta y \tag{8}$$

$$c_{11} = b_{11} \tag{9}$$

$$c_{02} = b_{02} \tag{10}$$

This function has six degrees of freedom and could be derived from six samples of the correlation function or the particle image. However, the use of a square number of samples is advantageous, due to the symmetry of available information around the maximum sample. Then, the six coefficients c_{ij} must be derived using a regression analysis. As a figure of merit, the minimum of the L_2 norm of the logarithmic intensity values:

$$L_2 = \sum_{i;j=-1}^{1} \left[c_{00} + c_{10}i + c_{20}i^2 + c_{01}j + c_{11}ij + c_{02}j^2 - \ln(z_{X+i;Y+j})\right]^2 \tag{11}$$

with the co-ordinates X and Y of the maximum sample can be used, where $\sum_{i;j=-1}^{1}$ means $\sum_{i=-1}^{1}\sum_{j=-1}^{1}$. This yields the coefficients:

$$c_{10} = \frac{1}{6}\sum_{i;j=-1}^{1} i\,\ln(z_{X+i;Y+j}) \tag{12}$$

$$c_{01} = \frac{1}{6}\sum_{i;j=-1}^{1} j\,\ln(z_{X+i;Y+j}) \tag{13}$$

$$c_{11} = \frac{1}{4}\sum_{i;j=-1}^{1} ij\,\ln(z_{X+i;Y+j}) \tag{14}$$

$$c_{20} = \frac{1}{6}\sum_{i;j=-1}^{1} (3i^2-2)\,\ln(z_{X+i;Y+j}) \tag{15}$$

$$c_{02} = \frac{1}{6}\sum_{i;j=-1}^{1} (3j^2-2)\,\ln(z_{X+i;Y+j}) \tag{16}$$

$$c_{00} = \frac{1}{9}\sum_{i;j=-1}^{1} (5-3i^2-3j^2)\,\ln(z_{X+i;Y+j}) \tag{17}$$

If individual weights $w_{i;j}$ of the intensity values $z_{i;j}$ are included, the L_2 norm becomes:

$$L_2 = \sum_{i;j=-1}^{1} w_{X+i;Y+j}\left[c_{00}+c_{10}i+c_{20}i^2+c_{01}j+c_{11}ij + c_{02}j^2-Z\right]^2 \tag{18}$$

with:

$$Z = \ln(z_{X+i;Y+j}) \tag{19}$$

and the coefficients can be derived as the solution of the system of linear equations:

$$\sum_{i;j=-1}^{1}\begin{pmatrix} i^2W & ijW & i^2jW & i^3W & ij^2W & iW \\ ijW & j^2W & ij^2W & i^2jW & j^3W & jW \\ i^2jW & ij^2W & i^2j^2W & i^3jW & ij^3W & ijW \\ i^3W & i^2jW & i^3jW & i^4W & i^2j^2W & i^2W \\ ij^2W & j^3W & ij^3W & i^2j^2W & j^4W & j^2W \\ iW & jW & ijW & i^2W & j^2W & W \end{pmatrix}\begin{pmatrix} c_{10} \\ c_{01} \\ c_{11} \\ c_{20} \\ c_{02} \\ c_{00} \end{pmatrix} = \sum_{i;j=-1}^{1}\begin{pmatrix} iWZ \\ jWZ \\ ijWZ \\ i^2WZ \\ j^2WZ \\ WZ \end{pmatrix} \tag{20}$$

with:

$$W = w_{X+i;Y+j} \tag{21}$$

The individual weights can be used, for example, to refine the influence of the appropriate pixels to the location estimation depending on the reliability of the intensity. For filtered or interpolated images, this can be used to avoid deviations at the edges of the images. Furthermore, the weight of correlation values at large displacements with higher estimation variance due to the smaller overlapping fraction of the interrogation areas can be accordingly reduced. Note that the weighting algorithm as introduced by Ronneberger et al. (1998) works differently and cannot be used here, since the logarithm of the intensity values introduces an additional bias, which is independent of the noise distribution.

From Eqs. 5, 6, 7, 8, 9, and 10, the co-ordinates of the maximum location can be derived as:

$$\Delta x = \frac{c_{11}c_{01}-2c_{10}c_{02}}{4c_{20}c_{02}-c_{11}^2} \tag{22}$$

$$\Delta y = \frac{c_{11}c_{10}-2c_{01}c_{20}}{4c_{20}c_{02}-c_{11}^2} \tag{23}$$

Additionally, the peak height can be derived as:

$$a = \exp\{c_{00}-c_{20}\Delta^2 x - c_{11}\Delta x\Delta y - c_{02}\Delta^2 y\} \tag{24}$$

3 Estimation accuracy

The two-dimensional Gaussian regression (nine-point regression) works excellently for Gaussian-shaped particle images or correlation peaks, circular or elliptical in any orientation. If the particle images or correlation peaks differ from the Gaussian shape, the systematic deviation of the particle position or displacement estimation becomes significant. For comparison with the two separate one-dimensional, three-point interpolations (2×3-point interpolation) a numerical simulation has been used. A series of images of single particles has been generated based on the Airy intensity function with varying particle image diameters (the first zero value of the Airy function) and particle center locations, integrated over a square pixel area of 1 pixel^2 size. The individual deviations of the position estimates have been summarized using the root mean square (RMS) bias, which is shown in Fig. 2a as a function of the simulated particle image diameter. In a second series of images, the photon noise has been simulated based on the Poisson distribution of the number of photons, where a number of 10,000 photons corresponds to the maximum intensity of the particle image. The results are shown in Fig. 2b.

For small particle images (<2 pixels diameter), both methods have significant systematic deviations because, here, the integrated Airy function differs from the Gaussian model of the interpolation or regression. For larger particle images (>3 pixels diameter), without the photon noise, the deviations of the two methods are comparable, and decrease for larger particle image diameters because the Airy function converges towards the assumed Gaussian shape. For the images with photon noise, the RMS bias increases with the particle image

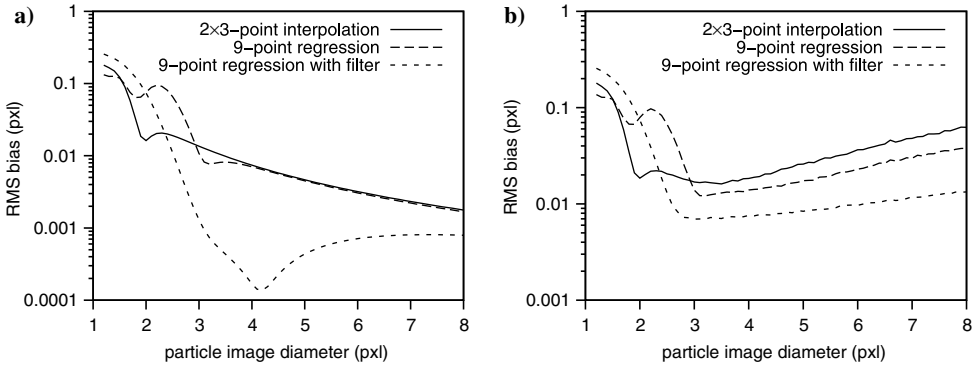

Fig. 2a, b Root mean square (RMS) bias of the one-dimensional three-point interpolation and the two-dimensional Gaussian regression: **a** without noise and **b** with simulated photon noise

diameter because the difference between the samples used for the interpolation or regression decreases, while the random fluctuations slightly increase (Prasad et al. 1992; Willert 1996; Westerweel 1997). However, the bias is smaller for the nine-point regression, since more information of the given image is used.

In the intermediate range between 2 and 3 pixels diameter, the bias of the nine-point regression is significantly larger than the bias of the 2×3-point interpolation. In this range, the additionally used image intensity values (nine instead of five samples), which differ from the assumed Gaussian shape, introduce an additional bias. To improve the situation, the image has been low-pass-filtered using a Gaussian filter, which has the advantage that the noise is significantly reduced and the particle image shape is changed towards a Gaussian profile. Additionally, the Gaussian filter can be used to down-sample or over-sample the image, so that the particle image or correlation peak width is optimized. If the low-pass filter yields too wide particle images for instance, the given procedure can be modified to use every second row and column of the image only. In the given case, a filter with an 11×11-point kernel and the coefficients:

$$c(i;j) = \exp\left[-0.5(i^2 + j^2)\right] \quad i;j = -5 \ldots 5 \tag{25}$$

has been used (Nobach et al. 2004), which significantly reduces the RMS bias for particle image diameters > 2.5 pixels in both cases, without and with the photon noise.

Note that this simulation used only circular particle images. In the case of elliptical and rotated particle images, only the nine-point regression yields reliable estimates of the particle positions, whereas the 2×3-point interpolation fails.

4 Experimental verification

To experimentally verify the algorithm, PIV images have been taken in a bubble column, where bubbles are rising in stagnant water. The principle of the measurement system is equivalent to that given by Lindken and Merzkirch (2002). The flow is seeded with fluorescent (Rhodamin B) particles with a diameter from 20 μm to 45 μm. The fluorescence is excited with a Nd-YAG laser light sheet and the bubble outlines are visualized with a back-light (808 nm) produced by a diode laser. The scattering of bubbles is blocked by an optical long-pass filter (> 560 nm) in order to capture only the fluorescing tracer particles and the shadows of bubbles with a CCD camera. The camera is equipped with a macro-objective lens (Navitar 7000) that produces strong aberrations in case of a magnification of 0.57 and a small aperture. Therefore, images of fluorescent particles are elliptically distorted and the background intensity of the image is high and variable.

Figure 3a shows the upper-left corner of an example image from this series, where the particle images are

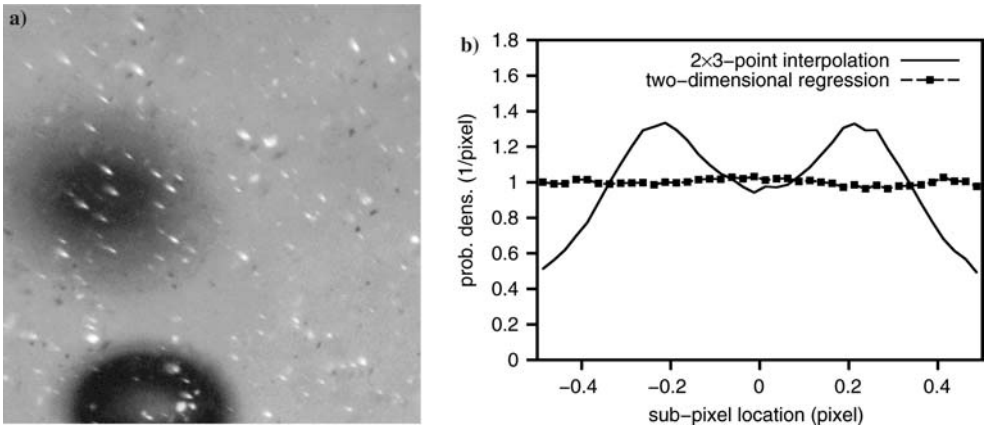

Fig. 3 **a** Upper-left corner of an experimental image of bubbles rising in stagnant water that is seeded with fluorescent tracer particles and **b** appropriate probability density function for the computed fractional part of the x component of particle positions

strongly distorted. After low-pass filtering according to Eq. 25, the particles have been detected by using a simple threshold. Then, the particle positions have been calculated with the given two-dimensional Gaussian fit method. The appropriate probability density functions for the sub-pixel estimation procedures of the particle locations are shown in Fig. 3b. A strong pixel locking can be seen for the two one-dimensional, three-point interpolations, while it is effectively reduced for the two-dimensional regressions. Note that, without the Gaussian low-pass filter, the pixel locking reduction is less effective, due to the non-Gaussian particle image shape. However, even with the Gaussian low-pass filter, a small pixel locking remains, because the Gaussian filter cannot completely correct the non-Gaussian image shape. Further sources of pixel locking are the high background intensity level (intensity offset) and the detectability of the particles depending on the sub-pixel location of the particles.

5 Summary

An explicit procedure has been introduced for the regression of a two-dimensional Gaussian function including rotated, elliptical particle image shapes. The advantage compared to the two separate, one-dimensional, three-point interpolations is that the explicit procedure avoids pixel locking in the case of elliptical, non-axially orientated particle images or correlation peaks. The capability of the two-dimensional Gaussian regression to significantly reduce the pixel locking has been verified using experimental images. Additionally, the estimation accuracy of the method in combination with a Gaussian low-pass filter has been investigated using numerical simulations. Since this procedure is explicit, it yields directly the required values without any iteration, which reduces the numerical calculation costs. Because the procedure cannot handle a constant offset value, a low noise intensity and an accurate removal of the background gray offset is required. Therefore, the performance of the given procedure stays between the two orthogonal one-dimensional Gaussian three-point interpolation and the two-dimensional Gaussian fit given by Ronneberger et al. (1998).

Acknowledgements The financial support of the Deutsche Forschungsgemeinschaft under grant Tr 194/21 and of the Finnish National Technology Agency, TEKES are gratefully acknowledged.

References

Adrian RJ, Yao CS (1985) Pulsed laser technique application to liquid and gaseous flows and the scattering power of seed materials. Appl Opt 24(1):44–52

Alexander BF, Ng KC (1991) Elimination of systematic error in sub-pixel accuracy centroid estimation. Opt Eng 30:1320–1331

Huang H, Dabiri D, Gharib M (1997) On error of digital particle image velocimetry. Meas Sci Technol 8:1427–1440

Keane RD, Adrian RJ (1992) Theory of cross-correlation analysis of PIV images. Appl Sci Res 49:191–215

Lindken R, Merzkirch W (2002) A novel PIV technique for measurements in multiphase flows and its application to two-phase bubbly flows. Exp Fluids 33:814–825

Lourenco I, Krothapalli A (1995) On the accuracy of velocity and vorticity measurements with PIV. Exp Fluids 18:421–428

Marxen M, Sullivan PE, Loewen MR, Jähne B (2000) Comparison of Gaussian particle center estimators and the achievable measurement density for particle tracking velocimetry. Exp Fluids 29:145–153

Morgan JS, Slater DC, Timothy JG, Jenkins EB (1989) Centroid position measurements and subpixel sensitivity variations with the MAMA detector. Appl Opt 28(6):1178–1192

Nobach H, Damaschke N, Tropea C (2004) High-precision sub-pixel interpolation in PIV/PTV image processing. In: Proceedings of the 12th international symposium on applications of laser techniques to fluid mechanics, Lisbon, Portugal, July 2004, paper 24.1

Prasad AK, Adrian RJ, Landreth CC, Offutt PW (1992) Effect of resolution on the speed and accuracy of particle image velocimetry interrogation. Exp Fluids 13:105–116

Roesgen T (2003) Optimal subpixel interpolation in particle image velocimetry. Exp Fluids 35:252–256

Ronneberger O, Raffel M, Kompenhans J (1998) Advanced evaluation algorithms for standard and dual plane particle image velocimetry. In: Proceedings of the 9th international symposium on applications of laser techniques to fluid mechanics, Lisbon, Portugal, July 1998, paper 10.1

Westerweel J (1997) Fundamentals of digital particle image velocimetry. Meas Sci Technol 8:1379–1392

Willert C (1996) The fully digital evaluation of photographic PIV recordings. Appl Sci Res 56(2–3):79–102

Willert CE, Gharib M (1991) Digital particle image velocimetry. Exp Fluids 10:181–193